Superconductivity in Ru-substituted polycrystalline $BaFe_{2-x}Ru_xAs_2$

Shilpam Sharma,[1] A. Bharathi,[1,*] Sharat Chandra,[2] V. Raghavendra Reddy,[3] S. Paulraj,[4] A. T. Satya,[1] V. S. Sastry,[1] Ajay Gupta,[3] and C. S. Sundar[1]

[1]*Condensed Matter Physics Division, Materials Science Group, Indira Gandhi Centre for Atomic Research, Kalpakkam 603102, India*

[2]*Materials Physics Division, Materials Science Group, Indira Gandhi Centre for Atomic Research, Kalpakkam 603102, India*

[3]*UGC-DAE Consortium for Scientific Research, Khandwa Road, Indore 452017, India*

[4]*Physics Department, Periyar University, Salem 636 011, India*

(Received 27 March 2009; revised manuscript received 19 April 2010; published 12 May 2010)

The occurrence of bulk superconductivity at ~22 K is reported in polycrystalline samples of $BaFe_{2-x}Ru_xAs_2$ for nominal Ru content in the range of $x=0.75-1.125$. A systematic suppression of the spin-density-wave transition temperature (T_{SDW}) precedes the appearance of superconductivity in the system. A phase diagram is proposed based on the measured T_{SDW} and superconducting transition temperature (T_C) variations as a function of Ru composition. Band-structure calculations indicate introduction of electron carriers in the system upon Ru substitution. The calculated magnetic moment on Fe shows a minimum at $x=1.0$, suggesting that the suppression of the magnetic moment is associated with the emergence of superconductivity. Results of low-temperature and high-field Mössbauer measurements are presented. These indicate weakening of magnetic interaction with Ru substitution.

DOI: 10.1103/PhysRevB.81.174512 PACS number(s): 74.10.+v, 74.25.Ha, 74.25.Jb, 74.62.Dh

I. INTRODUCTION

Over the last two years, much progress has been made in establishing superconductivity unambiguously in MFe_2As_2 (M=Ba, Sr, Ca, and Eu) systems.[1–6] The pristine sample that has a spin-density-wave (SDW) ground state is pushed into a superconducting (SC) state by electron/hole doping and application of pressure.[2,7–10] Band-structure calculations point to the fact that SDW state arises on account of the special two-dimensional geometry of Fermi surface that is unstable to nesting.[11,12] Also associated with or preceding the magnetic transition is a tetragonal to orthorhombic structural transition, which is suppressed in the superconducting state. The strong interplay of structure, magnetism, and electronic structure have been investigated recently in the Co-substituted $BaFe_{2-x}Co_xAs_2$ system.[13] The temperature composition phase diagrams determined for the different chemical substitutions at different sites in $BaFe_2As_2$ show a generic behavior as a function of the concentration of the substituent, that is, a systematic suppression of the SDW transition, followed by coexistence of SDW and SC and the occurrence of a superconducting dome.[14–16] Several transition-metal (TM) substitutions with electrons in excess of Fe, forming $BaFe_{2-x}TM_xAs_2$ compounds, have been studied but the maximum T_C has remained at ~25 K.[17] A much higher T_C of 38 and ~35 K was however observed by optimal hole doping in the $Ba_{1-x}K_xFe_2As_2$ system[2] and in $BaFe_2As_2$ by application of high pressure.[10] A systematic investigation on the role of hydrostatic pressure in the pressure-dependent resistivity study of $BaFe_2As_2$, has revealed that uniaxial pressure favors the occurrence of high T_C at 36 K whereas a lower T_C of 29 K occurs under truly hydrostatic pressure.[18] Consistent with this finding are results that indicate that strained crystals of $BaFe_2As_2$ and $SrFe_2As_2$ display superconductivity at ambient pressure.[19] A compilation of structural data from several compounds of the related ReOFeAs (Re=rare earth) superconducting family, indicates that T_C is optimized at a particular Fe-As distance[20] and/or at a particular Fe-As tetrahedral angle,[21] indicating that the local structure of the $FeAs_4$ tetrahedra plays a crucial role in determining T_C. Devising schemes to effect structural distortions by chemical substitution that would lead to higher T_C in the $BaFe_2As_2$ system will be useful.

Thus motivated, we examine the effect of Ru substitution at the Fe site in $BaFe_2As_2$. At the outset, it is clear that Ru is isoelectronic to Fe and being larger in size should introduce steric effects, affecting the Fe-As bond length leading to distortions of the $FeAs_4$ tetrahedral motifs. In addition, the larger radius of the 4d electron shell should increase the metal-metal overlap in the Fe/Ru layer and increase the hybridization of metal atom with As leading to significant alterations in the electronic structure. It is established that $BaRu_2As_2$ forms by solid-state reaction, is isostructural to $BaFe_2As_2$ and is metallic although nonsuperconducting,[22] indicating the feasibility of Ru substitution in $BaFe_2As_2$. In this paper, we report on the synthesis of polycrystalline samples of the $BaFe_{2-x}Ru_xAs_2$ series for various Ru fraction, x, and on investigations of their structural, magnetic, and superconducting properties. The study indicates a systematic suppression of the low-temperature SDW state with increase in Ru concentration, leading to the observation of superconductivity in $BaFe_{2-x}Ru_xAs_2$ at $x\sim1.0$, at ~20 K. Notably, at this composition, the magnetic moment at Fe is suppressed as verified by Mössbauer measurements and also supported by the magnetic moment per atom data from the full-potential total-energy calculations.

II. EXPERIMENTAL DETAILS

The $BaFe_{2-x}Ru_xAs_2$ (x=0.0, 0.25, 0.50, 0.75, 0.875, 1.0, 1.125, 1.25, and 1.5) samples were prepared by solid-state reaction from preformed FeAs and RuAs powders and Ba chunks under 30 bars Ar pressure.[23] After an initial heat treatment at 1233 K for 10 h, the reacted powder was

ground, pelletized, and sintered at 1173 K for 5 h. All weighing operations and loading of the reactants into the Ta crucibles were done in a helium-filled glove box. The FeAs and RuAs powders were prepared in the same setup by heat treating the intimate mixtures of Fe and As powders in quartz crucibles in the temperature range of 873–1073 K for 6 h. The procedure was repeated twice with an intermediate grinding. The samples were characterized for phase formation and crystal structure using a STOE diffractometer operating in the Bragg-Brentano geometry. The resistivity measurements, carried out in the four-probe geometry, were done in a dipper cryostat. The diamagnetism of the samples was confirmed by magnetization measurements in a CRYOGENIC, U.K. make liquid-helium-based vibrating sample magnetometer operating at 20.4 Hz. H_{C2} and the Hall-coefficient measurements were carried out in an exchange gas cryostat in the 6–300 K temperature range under magnetic fields up to 12 T. ^{57}Fe Mössbauer measurements were carried out in transmission mode with ^{57}Co radioactive source in constant acceleration mode using a standard personal computer based Mössbauer spectrometer equipped with a Weissel make velocity drive. The measurements were carried out at 300 and 5 K, and 5 T external magnetic field applied parallel to the gamma rays (using JANIS Super-OptiMag superconducting magnet). Velocity calibration of the spectrometer was done with natural iron absorber at room temperature.

III. RESULTS AND DISCUSSIONS

The x-ray diffraction (XRD) results indicate the formation of the $I4/mmm$, $ThCr_2Si_2$ structure for all Ru fractions substituted. A small fraction of impurity peaks due to Ru/Fe and Ba arsenides were identified. From Rietveld analysis of the XRD data obtained for the $x=0.875$ sample, the fractional z coordinate of arsenic (Z_{As}), transition-metal As bond length and the two ($e_{1,2}$) tetrahedral angles of $FeAs_4$ tetrahedron were determined to be 0.3554 nm, 0.2424 nm and 112.51°, 107.97°, respectively. The refined Ru composition was determined to be 0.864, which is close to the nominal composition. The tetrahedral angles are similar to those obtained in the case of isoelectronic substitution of P at As site for the optimal superconducting composition[16] but different from those seen under the application of pressure.[24]

The lattice-parameter variations obtained from XRD data as a function Ru concentration are shown in Fig. 1. It is clear from the figure that with Ru substitution there is an increase in the a-lattice parameter whereas the c-lattice parameter shows a decrease, leading to a decrease in the c/a ratio. There is an overall increase in the cell volume of ~1.18% for $x=1.0$. Similar changes were observed in the $SrFe_{2-x}Ru_xAs_2$ system.[25] The changes in the cell parameters due to Ru substitution contrasts with the variations obtained in Co- and P-substituted $BaFe_2As_2$ and that under the application of pressure,[16,24,26] where a monotonic decrease in cell volume arises as a consequence of a decrease in both the a- and c-lattice parameters. In the $Ba_{1-x}K_xFe_2As_2$ system, while the a-lattice parameter decreases and c-lattice parameter increases, the cell volume remains constant with substitution.[27]

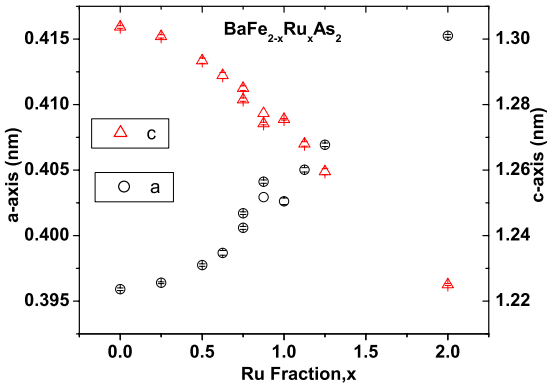

FIG. 1. (Color online) Variation in the a- and c-lattice parameters as a function of Ru fraction substituted.

The temperature dependence of resistivity normalized to the room-temperature value obtained in all Ru-substituted samples is shown in various panels in Fig. 2. The well-known drop in resistivity corresponding to the SDW transition[1] seen in $BaFe_2As_2$ is clearly visible at ~150 K in the $x=0.0$ sample. With increasing Ru substitution, for $x=0.25$, 0.50, and 0.625, the room-temperature resistivity decreases and the SDW transition shifts to a lower temperature. The onset of the SDW transition for the different Ru compositions are marked by " *" in the figure. For a Ru fraction of $x=0.75$, a small bump due to the SDW transition is seen. In addition, the resistivity in this sample shows a clear signature of the occurrence of a superconducting transition with an onset of 22 K, leading to zero resistance. This transition to the superconducting state is clearly seen in samples with Ru fraction of $x=0.875$, 1.0, and 1.125 but the anomaly due to SDW transition is not observed in them. The normal-state resistance in these superconducting samples indicates a linear T dependence up to 250 K. Further for the $x=0.625$ and 1.25 samples, although a fall in $R(T)/R(300\ K)$ is observed, no zero resistance is seen, and in the sample with $x=1.5$, no drop in resistivity is observed. It can be seen from the figure

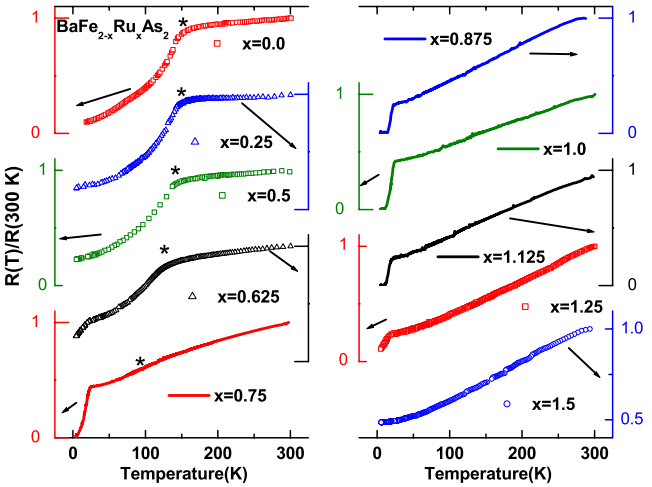

FIG. 2. (Color online) Variation in normalized resistivity with temperature in $BaFe_{2-x}Ru_xAs_2$ for various nominal Ru fractions, x, as indicated. The origin is shifted for each composition for clarity. The SDW transitions are indicated by stars.

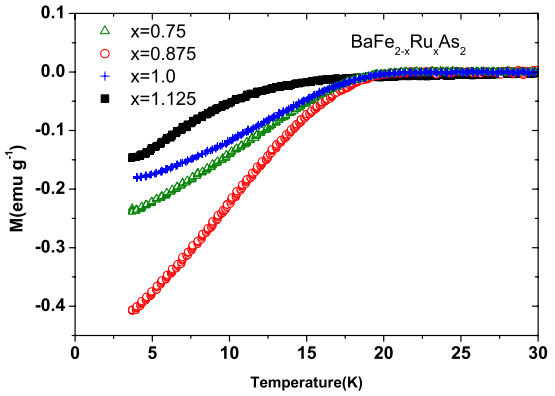

FIG. 3. (Color online) dc magnetization as a function of temperature for nominal $x=0.75$, 0.875, 1.0, and 1.125.

that the normal-state resistivity acquires curvature for $x=1.25$ and 1.5 samples. For these samples, the $R(T)$ in the normal state was seen to fit to a T^n power law with $n\sim 1.5$. Similar composition-dependent changes in the power-law behavior of the normal-state $R(T)$ were seen in the $BaFe_2As_{2-x}P_x$ system[16] and under the application of pressure.[10] The zero-field-cooled magnetization data of the four samples with Ru fraction $x=0.75-1.125$ sample is shown in Fig. 3. The diamagnetic drop at ~ 20 K is evident from the data for samples with x in the range of $x=0.75-1.125$. No diamagnetic signals were observed for samples with $x=0.625$ and 1.25. The presence of zero resistance (Fig. 2) and diamagnetism (Fig. 3) in the samples with Ru composition in the composition range of $x=0.75-1.125$ provides unambiguous evidence for observance of superconductivity in the $BaFe_{2-x}Ru_xAs_2$ system in this composition regime.

The variation in resistivity with temperature for the sample with a Ru fraction of $x=0.875$, measured under various fields upto 12 T is shown in Fig. 4. A systematic decrease in the superconducting onset with increasing magnetic field is clearly seen. Broadening of the superconducting transi-

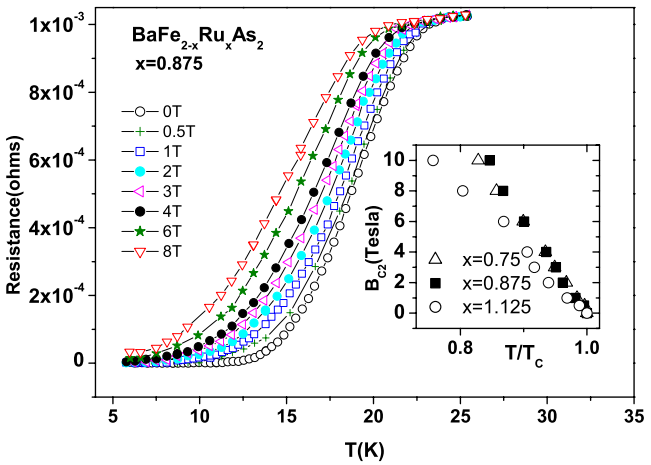

FIG. 4. (Color online) The variation in the SDW transition temperatures and superconducting onsets as a function nominal Ru fraction x. SDW and superconductivity states coexist for the $x=0.75$ sample.

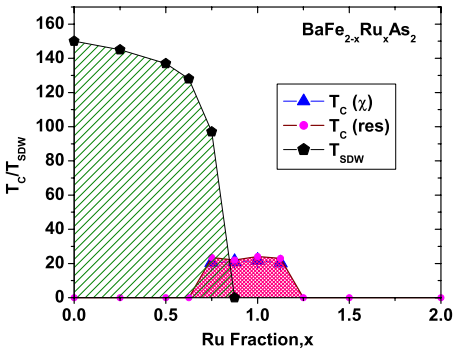

FIG. 5. (Color online) Variation in resistance versus temperature for various external magnetic fields indicated, for Ru fraction, $x=0.875$. Inset shows the field dependence of superconducting transition temperatures, normalized to their zero-field counterparts, for $x=0.75$, 0.875, and 1.125.

tions upon the application of magnetic field is negligible indicating the minor role of anisotropy and granularity in this system. This behavior is similar to the results that are obtained for the superconducting $Ba_{1-x}K_xFe_2As_2$ and $BaFe_{2-x}Co_xAs_2$ compounds.[23,26] A linear fit to the onset data resulted in the evaluation of $-dH_{C2}/dT$ at T_C to be 2 T/K. This value is close to that obtained for Co substitution in $Ba(Fe_{1-x}Co_x)_2As_2$ for $x=0.034$ and 0.07 (Ref. 26) but is substantially smaller than the value of ~ 7 T/K (Ref. 23) seen in K-substituted samples having a T_C of 38 K. The variation in the critical field versus normalized T_C $[T_C(B)/T_C(0)]$ are compared for the three superconducting samples with varying Ru compositions in the inset of Fig. 4.

In Fig. 5, we summarize the variation in T_{SDW} and T_C obtained from the resistivity curves shown Fig. 2, as a function of Ru concentration. Data for samples that exhibit zero resistivity are only included in this figure. The superconducting onsets obtained from magnetization (Fig. 3) are also shown in the figure. It is evident from the figure that the SDW transition temperature decreases from that in the pristine compound for Ru fractions up to $x=0.75$. Coexistence of SDW and SC seems to occur in the $x=0.75$ sample. It is clear from Fig. 5 that for Ru fractions of $x=0.875$, 1.0, and 1.125, only the superconducting phase is stabilized. Superconductivity is absent for Ru concentration greater than or equal to $x=1.25$.

To investigate how Ru substitution affects the electronic structure, we have performed spin-polarized density-functional calculations for $BaFe_2As_2$, $BaFe_{1.5}Ru_{0.5}As_2$, $BaFe_{1.0}Ru_{1.0}As_2$, $BaFe_{0.50}Ru_{1.5}As_2$, and $BaRu_2As_2$, using the full-potential linearized plane wave plus localized orbitals method, with the WIEN2K code[27] and the results are shown in Fig. 6. The details of the calculation are elaborated in Ref. 28. The calculations were carried out using a superstructure, obtained by the $\sqrt{2}\times\sqrt{2}\times 1$ construction from the ground-state-relaxed crystal structure of $BaFe_2As_2$ already published in literature,[29,30] as shown in Fig. 6(c) [$\mathbf{a}'=(\mathbf{a}+\mathbf{b})$, $\mathbf{b}'=(\mathbf{a}-\mathbf{b})$, $\mathbf{c}'=\mathbf{c}$; $\mathbf{a}$, $\mathbf{a}'$, etc., are the real-space lattice vectors of the original and the transformed structures, respectively]. In this reconstructed structure, all the four Fe atoms occupy nonequivalent sites. The experimental lattice parameters of the

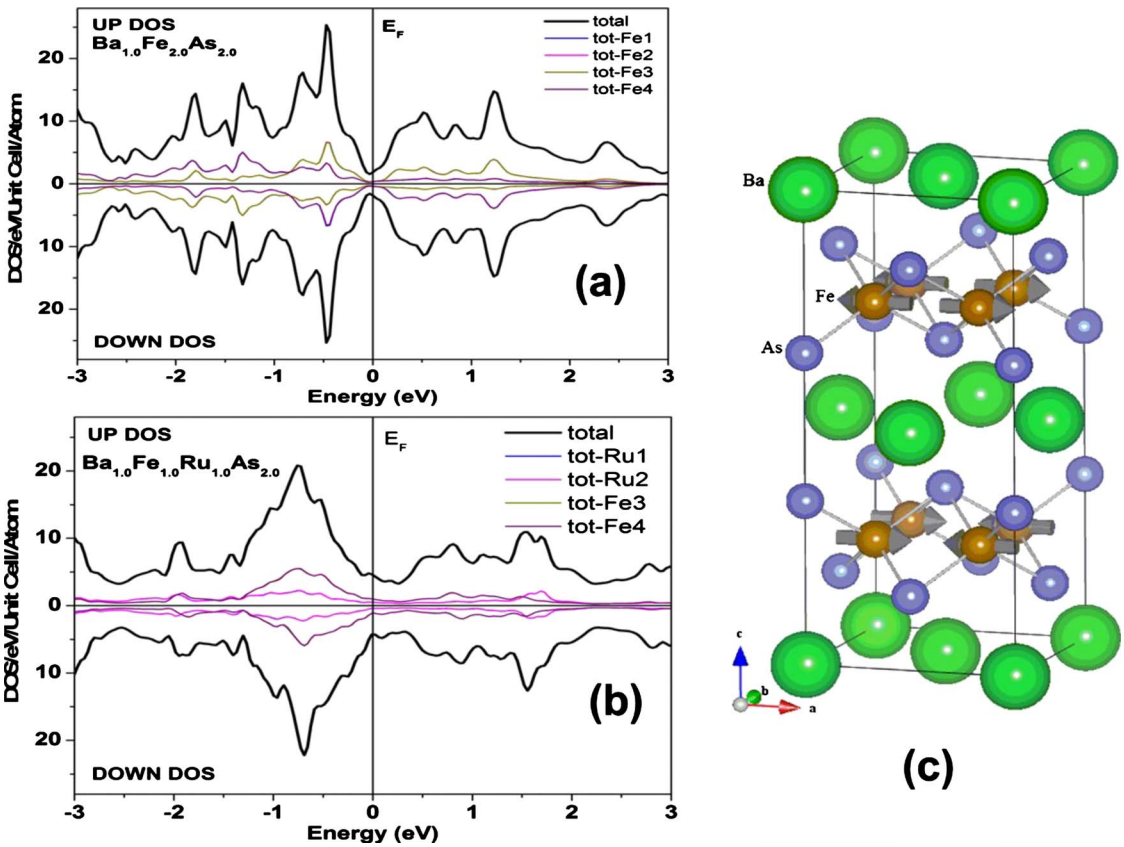

FIG. 6. (Color online) A comparison of the spin-polarized density of states obtained from first-principles calculations in (a) $BaFe_2As_2$ and (b) $BaFe_{1.0}Ru_{1.0}As_2$. (c) A schematic of the structure of the superstructure used in the calculations.

Ru fraction of $x=0.5$, 1.0, and 2.0 were used for the Ru-substituted electronic-structure calculations. The calculated density of states (DOS), shown in Fig. 6(a) for $BaFe_2As_2$, is in agreement with that obtained earlier.[29] The atom-resolved DOS for *d* Fe and *p* As are also indicated in the figure. The Ba atom does not contribute appreciably to the DOS near the Fermi level (E_F). A steady increase in DOS at E_F was seen with increase Ru substitution. This is clear from Fig. 6(b), where with 50% Ru substitution, the DOS at E_F increases to 4.40 eV/unit cell/atom from 1.82 eV/unitcell/atom in the $BaFe_2As_2$ [Fig. 6(a)], implying a change in the local hybridization characteristics as Ru is isovalent to Fe in this system. A similar increase in DOS at E_F has been observed for the $BaFe_2As_2$ system under the application of pressure and with K doping.[24] The significant broadening and their increased contribution to DOS suggests that the Fe 3*d* electrons get delocalized with Ru substitution. Ru *d* levels also contribute to a small extent to the DOS at E_F. The converged E_F for $BaFe_2As_2$ is 0.60268 Ry while that for $BaFe_{1.5}Ru_{0.5}As_2$ is 0.63645 Ry. Thus the upward shift in E_F with increasing Ru content implies an electron doping due to Ru substitution.

To check on the nature of carriers introduced due to Ru substitution, Hall-coefficient measurements were carried out in the 10–300 K temperature range in a home built setup in the van der Pauw geometry.[31] The R_H versus *T* for the single-crystalline sample of $BaFe_2As_2$ and the R_H versus temperature on the polycrystalline $BaFe_{2-x}Ru_xAs_2$ for the nominal $x=0.75$ sample are displayed Figs. 7(a) and 7(b), respec-

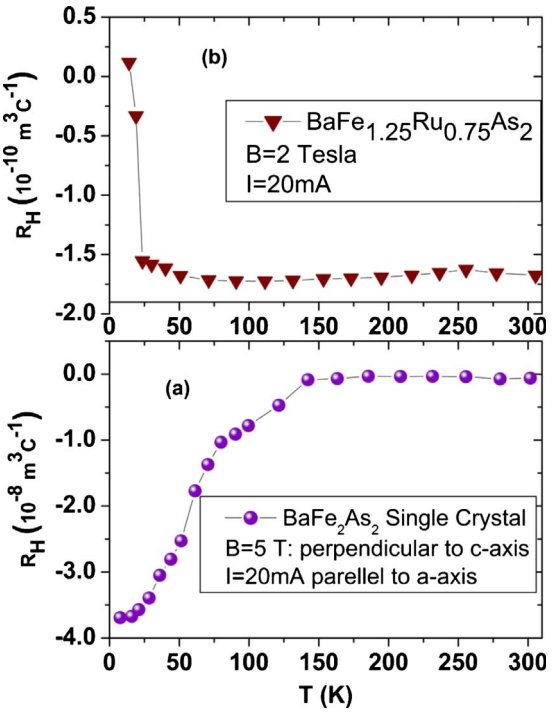

FIG. 7. (Color online) Plots of the Hall coefficient in (a) $BaFe_2As_2$ single crystals and (b) in polycrystalline $BaFe_{2-x}Ru_xAs_2$ for $x=0.75$; the measuring field and current used in the experiments are indicated.

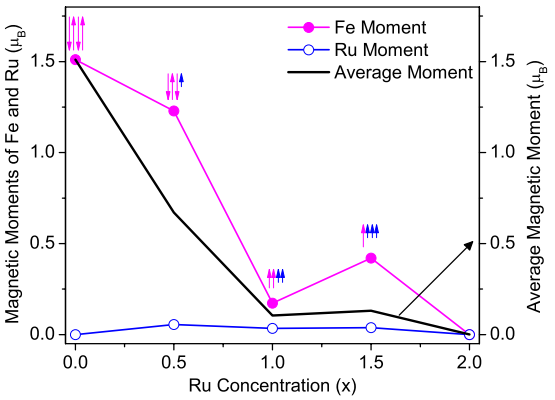

FIG. 8. (Color online) The variations in the maximum magnetic moment and the averaged magnetic moment with increase in Ru concentration as obtained from spin-polarized calculations. The arrows indicate the directions and magnitude of the magnetic moment at the four distinct sites in a Fe/Ru plane of the supercell obtained from the calculations.

tively. Both the magnitude and temperature dependence of the Hall coefficient shown in Fig. 7(a) are in agreement with earlier reports on single crystals[32] of $BaFe_2As_2$. From Fig. 7(b), it is clear that the R_H is negative in the normal state of the superconducting, Ru-substituted sample. The R_H values also show the characteristic drop to zero due to occurrence of superconductivity below ~20 K. The R_H value in the normal state of the Ru-substituted sample shown in Fig. 7(b) is smaller than that seen in $Ba_{0.65}K_{0.45}Fe_2As_2$ and that in the $BaFe_{1.8}Co_{0.2}As_2$ systems[8,31] and is temperature independent. Assuming a one-band model, this small R_H translates to an electron density, which is approximately ten times as large as that evaluated for the $BaFe_{1.8}Co_{0.2}As_2$ sample.[8]

Band-structure calculations were also used to evaluate the evolution of the magnetic state of $BaFe_2As_2$ as a function of Ru substitution. For the $x=0.0$ and 0.5 structures, the lowest energy occurs for the stripe antiferromagnetic order[30] and for the $x=1.0$ and 1.5 superstructures, the lowest-energy configuration turns out to be paramagnetic. The magnetic moments of the Fe/Ru atoms were obtained from unconstrained minimization of total energy during the self-consistent iterations in the spin-polarized calculations. It was seen that the Ru atoms always align antiferromagnetically to the Fe atoms and only in the presence of the Fe atoms, do they show a very small magnetic moment. Also, Ba and As atoms always remain nonmagnetic. Essentially, Ru atoms also like to remain nonmagnetic in this structure. In the $x=0.5$ and 1.5 compositions, there are three Fe(Ru) atoms for one Ru(Fe) whereas for $x=1.0$, there are two Fe atoms for two Ru. Due to this inherent magnetic disorder present in the $x=0.5$ and 1.5 compositions, the magnetic moments obtained for all the Fe(Ru) atoms in the unit cell are different. The variations in the magnitude of the maximum of Fe/Ru moment and the averaged Fe/Ru magnetic moment are shown in Fig. 8. Also shown in the figure, is the sign of the magnetic moment at each Fe site in a Fe/Ru plane, as obtained from calculations. Two points clearly emerge from this figure: (1) the average magnetic moment decreases with increase in Ru and (2) the antiferromagnetic alignment is preferred only for the $x=0.0$ and 0.5 compositions. A small contribution from the Ru magnetic moment is also evident from Fig. 8. The Ru atoms in $BaRu_2As_2$ show zero magnetic moments.

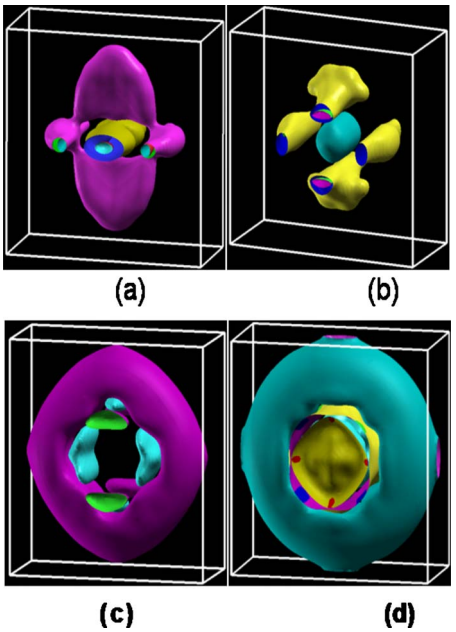

FIG. 9. (Color online) Evolution of the Fermi surface obtained from spin-polarized DFT calculations for the spin-up bands in $BaFe_{2-x}Ru_xAs_2$ for (a) $x=0.0$, (b) $x=0.5$, (c) $x=1.0$, and (d) $x=2.0$.

Figure 9 displays the evolution of the Fermi surface with Ru substitution, as obtained from band-structure calculations for the spin-down bands. The three-dimensional Fermi surfaces have been plotted for the $\sqrt{2}\times\sqrt{2}\times1$ superstructure. The Fermi surfaces for the original structure[29] can be obtained from these by the corresponding transformation for the reciprocal space [$\mathbf{a}^*=-(\mathbf{b}'^*+\mathbf{a}'^*)$, $\mathbf{b}^*=(\mathbf{b}'^*-\mathbf{a}'^*)$, $\mathbf{c}^*=\mathbf{c}'^*$; $\mathbf{a}^*$, $\mathbf{a}'^*$, etc., are the reciprocal-lattice vectors of the original and the transformed reciprocal space, respectively]. The spin-up bands also show similar features in all the cases, except for $x=0.5$. A few points to mention on careful perusal of Fig. 9 are (i) the Fermi surfaces become more connected with increase in Ru content, suggestive of increased delocalization of the carriers at E_F. (ii) Fermi surfaces for spin-up and spin-down electrons become very similar with increase in Ru content, suggesting a preference for a paramagnetic ground state for a substantial increase in Ru content, (iii) the Fermi surface gets larger, indicating electron addition due to Ru substitution, and (iv) nesting decreases with increasing Ru content, as is evident from the absence of the flat portions in the Fermi-surface plots.

To experimentally investigate the magnetic moment at the Fe site, Mössbauer measurements were carried out on the $x=0.0$, 0.5, and 1.0 samples at 5 K. The Mössbauer data for these samples obtained at 5 K are displayed in Fig. 10. The Mössbauer data displayed for the $x=0.0$ and 0.5 samples [Figs. 10(a) and 10(b)], show the characteristic six finger pattern due to magnetic ordering in the spin-density-wave state of the samples at 5 K. The magnetic hyperfine split data is analyzed with NORMOS-DIST program[33] and the data of

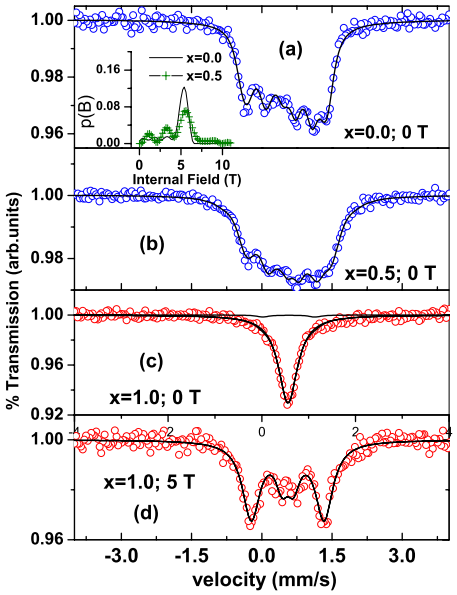

FIG. 10. (Color online) Variation in the transmitted intensity versus the velocity of the Mössbauer spectra measured at 5 K in $BaFe_{2-x}Ru_xAs_2$ samples with (a) $x=0.0$, (b) $x=0.5$, (c) $x=1.0$, and (d) $x=1.0$ with an external magnetic field of 5 T. Inset in (a) shows the probability distribution of the magnetic field for $x=0.0$ and 0.5 samples, obtained from fits of the corresponding data shown in (a) and (b).

superconducting sample is analyzed with NORMOS-SITE program.[33] The hyperfine magnetic split spectrum is fitted to a distribution of fields for $x=0$ and 0.5 samples as shown by solid lines in the figure. The probability distribution of hyperfine fields obtained from the fits, for the $x=0.0$ and 0.5 samples are shown in the inset of Fig. 10(a). It is clear from the figure that the hyperfine field distribution has a maximum at a field of ~5 T in the pristine sample and it becomes more spread out in the Ru containing sample with $x=0.5$. The observed value of average hyperfine field (BHF) for $x=0$ sample matches closely with that obtained earlier.[1,34] The Mössbauer spectrum of $x=1.0$ sample shown in Fig. 10(c) shows a broad singlet which is similar to that reported in K-substituted samples which show superconductivity at 38 K.[34] The fitted data of Fig. 10(c) has an isomer-shift value of 0.55 ± 0.01 mm/s corresponding to superconducting phase and a doublet with the hyperfine parameters matching with the $FeAs_2$ impurity phase.[35] The fraction of the $FeAs_2$ phase is estimated to be about ~3.5%. Figure 10(d) shows the Mössbauer spectrum of $x=1.0$ sample measured at 5 K and 5 T external magnetic field. The fact that the observed effective BHF (internal field) value is close to that of applied external magnetic field, within experimental errors, indicates that there is no magnetic ordering present in the $x=1.0$ sample. The Mössbauer results thus indicate that the magnetic interactions due to the SDW phase weaken with Ru substitution and are altogether absent in the superconducting sample with Ru composition of $x=1.0$.

It will be instructive to compare the phase diagrams determined from our study for the $BaFe_{2-x}Ru_xAs_2$ system with those of other systems belonging to the $BaFe_2As_2$ class. Coexistence of SDW and SC phases, occur in all the phase diagrams irrespective of how the phase changes are induced, i.e., by pressure or substitution, isoelectronic or otherwise. Our study indicates that optimal T_C occurs for Ru concentration between 0.75 and 0.875. This is similar to the isoelectronic substitution cases, of $BaFe_2As_{2-x}P_x$ and $SrFe_{2-x}Ru_xAs_2$, in which that optimal superconductivity occurs for $x \sim 0.8$. Whereas, it contrasts with optimal T_C being observed at $x \sim 0.2$ in the more extensively studied, $BaFe_{2-x}TM_xAs_2$ systems[17] in which the TM atoms add extra electrons as compared to Fe. This difference emphasizes the fact that to effect the electronic-structure change conducive for superconductivity a much larger distortion of the lattice is required for the case of isoelectronic substitution.

IV. SUMMARY AND CONCLUSIONS

Polycrystalline samples of $BaFe_{2-x}Ru_xAs_2$ samples have been synthesized by solid-state reaction from the FeAs, RuAs powders, and Ba chunks under 30 bars argon pressure. Resistivity, dc magnetization, Hall-coefficient, and Mössbauer measurements were employed to characterize the physical properties of the series. A phase diagram is proposed that indicates that the spin-density-wave ground state gives way to the occurrence of superconductivity in the x range of 0.75–1.125. Hall-coefficient measurements indicate introduction of electron carriers due to Ru substitution. Mössbauer results indicate a systematic suppression of the low-temperature magnetic state with increase in Ru content. Electron doping and magnetic-moment suppression with Ru substitution are supported by the total-energy and band-structure calculations.

ACKNOWLEDGMENTS

The authors are deeply indebted to Y. Hariharan, a former member of the group, for elaborate discussions and critical reading of the manuscript. S. Paulraj acknowledges financial support from UGC-DAE CSR and C. Sekar of Periyar University Salem, for his encouragement during this work.

*Corresponding author. FAX: ++91 44 27480081; bharathi@igcar.gov.in

[1] M. Rotter, M. Tegel, D. Johrendt, I. Schellenberg, W. Hermes, and R. Pottgen, Phys. Rev. B **78**, 020503(R) (2008).
[2] M. Rotter, M. Tegel, and D. Johrendt, Phys. Rev. Lett. **101**, 107006 (2008).
[3] K. Sasmal, B. Lv, B. Lorenz, A. M. Guloy, F. Chen, Y. Y. Xue, and C. W. Chu, Phys. Rev. Lett. **101**, 107007 (2008).
[4] Z. Ren, Z. Zhu, S. Jiang, X. Xu, Q. Tao, C. Wang, C. Feng, G. Cao, and Z. Xu, Phys. Rev. B **78**, 052501 (2008).

[5] H. S. Jeevan, Z. Hossain, D. Kasinathan, H. Rosner, C. Geibel, and P. Gegenwart, Phys. Rev. B **78**, 092406 (2008).
[6] M. S. Torikachvili, S. L. Bud'ko, N. Ni, and P. C. Canfield, Phys. Rev. Lett. **101**, 057006 (2008).
[7] N. Ni, S. L. Bud'ko, A. Kreyssig, S. Nandi, G. E. Rustan, A. I. Goldman, S. Gupta, J. D. Corbett, A. Kracher, and P. C. Canfield, Phys. Rev. B **78**, 014507 (2008).
[8] A. S. Sefat, R. Jin, M. A. McGuire, B. C. Sales, D. J. Singh, and D. Mandrus, Phys. Rev. Lett. **101**, 117004 (2008).
[9] P. L. Alireza, Y. T. C. Ko, J. Gillett, C. M. Petrone, J. M. Cole, G. G. Lonzarich, and S. E. Sebastian, J. Phys.: Condens. Matter **21**, 012208 (2008).
[10] A. Mani, N. Ghosh, S. Paulraj, A. Bharathi, and C. S. Sundar, EPL **87**, 17004 (2009).
[11] D. J. Singh, Physica C **469**, 418 (2009).
[12] D. Kasinathan, A. Ormeci, K. Koch, U. Burkhardt, W. Schnelle, A. Leithe-Jasper, and H. Rosner, New J. Phys. **11**, 025023 (2009).
[13] S. Nandi, M. Kim, A. Kreyssig, R. Fernandes, D. Pratt, A. Thaler, N. Ni, S. Bud'ko, P. Canfield, J. Schmalian, R. McQueeney, and A. Goldman, Phys. Rev. Lett. **104**, 057006 (2010).
[14] D. Johrendt and R. Poettgen, Physica C **469**, 332 (2009).
[15] J.-H. Chu, J. G. Analytis, C. Kucharczyk, and I. R. Fisher, Phys. Rev. B **79**, 014506 (2009).
[16] S. Jiang, H. Xing, G. Xuan, C. Wang, Z. Ren, C. Feng, J. Dai, Z. Xu, and G. Cao, J. Phys.: Condens. Matter **21**, 382203 (2009).
[17] P. Canfield and S. Bud'ko, arXiv:1002.0858, Condens. Matter Phys. (to be published).
[18] W. Duncan, O. Welzel, C. Harrison, X. Wang, X. Chen, F. Grosche, and P. Niklowitz, arXiv:0910.4267 (unpublished).
[19] J. S. Kim, T. D. Blasius, E. G. Kim, and G. R. Stewart, J. Phys.: Condens. Matter **21**, 342201 (2009).
[20] Y. Mizuguhci, Y. Hara, K. Deguchi, S. Tsuda, T. Yamaguchi, K. Takeda, H. Kotegawa, H. Tou, and Y. Takano, arXiv:1001.1801 (unpublished).
[21] K. Ishida, Y. Nakai, and H. Hosono, J. Phys. Soc. Jpn. **78**, 062001 (2009).
[22] R. Nath, Y. Singh, and D. C. Johnston, Phys. Rev. B **79**, 174513 (2009).
[23] A. Bharathi S. Shilpam Sharma, S. Paulraj, A. T. Satya, Y. Hariharan, C. S. Sundar, Physica C **470**, 8 (2010).
[24] S. A. J. Kimber, A. Kressig, Y. Z. Zhang, H. O. Jeschke, R. Valenti, F. Yokaichiya, E. Colombier, J. Yan, T. C. Hansen, T. Chatterji, R. J. McQueeney, P. C. Canfield, A. I. Goldman, and D. N. Argyriou, Nat. Mater. **8**, 471 (2009).
[25] W. Schnelle, A. Leithe-Jasper, R. Gumeniuk, U. Burkhardt, D. Kasinathan, and H. Rosner, Phys. Rev. B **79**, 214516 (2009).
[26] N. Ni, M. E. Tillman, J.-Q. Yan, A. Kracher, S. T. Hannahs, S. L. Bud'ko, and P. C. Canfield, Phys. Rev. B **78**, 214515 (2008).
[27] P. Blaha, K. Schwarz, G. K. H. Madsen, D. Kvasnicka, and J. Luitz, *WIEN2k, An Augmented Plane Wave Plus Local Orbitals Program for Calculating Crystal Properties*, edited by Karlheinz Schwarz (Techn. Universitat Wien, Austria, 2001).
[28] The generalized gradient approximation (PBE96) was used for the exchange interaction. The calculations were done with 1000 k points in the full Brillouin zone and $R^*_{\mathrm{MT}}K_{\mathrm{max}}$ was 12 for all the calculations. The ground-state-relaxed structure was obtained using the same method reported previously in literature (Ref. 29) for the same structure. The muffin-tin radii used were $2.2a_0$ for Ba and $2.1a_0$ for Fe, Ru, and As, where a_0 is the Bohr radius (Ref. 29). The calculation was converged with respect to the energy, charge displacement, and forces to the tune of 10^{-6} Ry, 10^{-6} bohr, and 1 mRy/bohr.
[29] D. J. Singh, Phys. Rev. B **78**, 094511 (2008).
[30] Q. Huang, Y. Qiu, W. Bao, M. A. Green, J. W. Lynn, Y. C. Gasparovic, T. Wu, G. Wu, and X. H. Chen, Phys. Rev. Lett. **101**, 257003 (2008).
[31] Shilpam Sharma,A. Bharathi, Y. Hariharan, and C. S. Sundar, Proceedings of DAE Solid State Physics Symposium, India, 2008 (unpublished), Vol. 53, p. 917.
[32] C. Zentile, J. Gillett, S. Sebastian, and J. Cooper, arXiv:0911.1259 (unpublished).
[33] R. A. Brand, NORMOS (Universitaet Duisburg, 1990).
[34] I. Nowik and I. Felner, Physica C **469**, 485 (2009).
[35] I. Felner I. Nowik, B. L. Joshua, H. Tapp, Z. Tang and A. M. Guloy, Hyperfine Interact. **191**, 61 (2009).